Journal of Photochemistry and Photobiology A: Chemistry 353 (2018) 53–64

Contents lists available at ScienceDirect

Journal of Photochemistry and Photobiology A: Chemistry

journal homepage: www.elsevier.com/locate/jphotochem

Invited feature article

Efficient non-doped bluish-green organic light emitting devices based on N_1 functionalized star-shaped phenanthroimidazole fluorophores

Jairam Tagare[a], Hidayath Ulla[b], M.N. Satyanarayan[b], Sivakumar Vaidyanathan[a,*]

[a] Optoelectronic Laboratory, Department of Chemistry, National Institute of Technology, Rourkela, India
[b] Optoelectronics Laboratory, Department of Physics, National Institute of Technology, Surathkal, India

ARTICLE INFO

Article history:
Received 7 September 2017
Received in revised form 25 October 2017
Accepted 3 November 2017
Available online 6 November 2017

Keywords:
DFT
Fluorescence
TPA
Non-doped organic light emitting diodes

ABSTRACT

In this paper, two star-shaped fluorescent phenanthroimidazole fluorophores, tris(4-(1-(3-(trifluoromethyl)phenyl)-1H-phenanthro[9,10-*d*]imidazol-2-yl)phenyl)amine (PIMCFTPA) and tris(4-(1-(4-(trifluoromethyl)phenyl)-1H-phenanthro[9,10-*d*]imidazol-2-yl)phenyl)amine (PIPCFTPA) with a D–π–A structure were designed and synthesized by attaching a hole-transporting triphenylamine and an electron transporting phenanthroimidazole moiety. A detailed photophysical, thermal, electrochemical and related properties were systematically studied. Furthermore, theoretical investigations (DFT) were performed to get a better understanding of the electronic structures. In particular, PIMCFTPA shows blue shifted emission due to the most twisted conformation and reduced intermolecular interaction as compared with PIPCFTPA. Both the fluorophores exhibit high glass transition temperatures and high thermal stabilities with decomposition temperatures up to 377 °C. The excellent stability renders them promising materials in electroluminescent devices. Non-doped organic light-emitting devices (OLEDs) using these fluorophores as emissive materials display bluish green emissions with high efficiency (6.58 cdA^{-1}, 5.91 lmW^{-1}, 3.62% at 100 cdm^{-2}), low turn-on voltages (2.83 V) (PIMCFTPA) and excellent spectral stability. Our results suggest that the molecular design strategy of integrating TPA with phenthroimdazole play an important role in the device performance.

1. Introduction

Organic materials applicable in organic light-emitting diodes (OLEDs) have attracted wide attention since the breakthrough work of Tang and Van Slyke because of their potential applications in full-color displays and lighting applications [1,2]. For realizing these applications, it is essential to have the three primary colors, red, green and blue (RGB) [3–6]. Though a large number of efficient red and green emitters have been reported in recent years, [7] the progress in highly efficient blue emitters has remained a formidable challenge to date [8–10]. Due to their inherent wide energy band-gaps, blue emitters possess limited delocalization which hampers the electron injection into the emitting layer [11]. In this context, highly efficient blue materials are considered as promising substitutes to promote the commercialization of OLEDs. Significant efforts have been made to design versatile blue materials aiming at further improving device efficiency, chromaticity and lifetime. Spin-statistics state that 75% of triplet excitons and 25% of singlet excitons are generated by the recombination of electrons and holes in organic semiconductor materials. By harvesting both singlet and triplet excitons through intersystem crossing, phosphorescent OLEDs (PhOLEDs) approach 100% internal quantum efficiency (IQE), however, in fluorescent OLEDs, the IQE is limited to 25% due to the deactivation of triplet excitons [12–14]. Although PhOLEDs have reached their IQE limit [15], they have some disadvantages, including lower electroluminescence (EL) efficiency under high current densities [16], rather low reliability in the blue region of the visible spectrum for practical applications and more expensive. Fluorescent OLEDs have continued to attract interest because of their long operational lifetimes, high colour purity of EL and potential to be manufactured at low cost in next-generation full-colour display and lighting applications. Most blue EL devices reported previously involve the use of dopants. However, to achieve an optimized device performance, careful control of the dopant concentration is required [17]. On the other hand, performance degradation due to phase separation upon heating is also a problem encountered in these devices [18–20]. To overcome these disadvantages, the fabrication of non-doped fluorescent OLED device has been attracting considerable attention and these devices have exhibited a high external quantum

* Corresponding author.
E-mail address: vsiva@nitrkl.ac.in (S. Vaidyanathan).

https://doi.org/10.1016/j.jphotochem.2017.11.001
1010-6030/

efficiency [21–23]. Also, by balancing the transport of charge carriers, the OLED efficiency could be improved [24–27].

Recently some blue fluorophores with high luminescent efficiency based on pyrene, anthracene, phosphine oxide, fluoranthene, pyrazolo-quinoline, oxadiazoles, naphthalimide and imidazole have been developed [28–40]. However, phenanthroimidazole continue to show considerable interest in organic electronics, due to ease in fluorophore modification at N_1 and C_2 position. On the other hand, these materials have the rigid skeleton, show high carrier mobilities, high thermal stability, as well as good film forming ability, leading to promising applications as blue emitters in high-performance OLEDs [41–47]. In general, hole mobility is higher than that of the electron mobility in the device [48]. From the available literature, one can conclude that the reported phenanthroimidazole based molecules are mainly having shape of linear and bent (consist of both charges transporting moieties) [49–51]. Nevertheless, so far, triphenylamine decorated star shaped phenanthroimidazole molecules have not been reported. We made an attempt to incorporate the three electron deficient (phenanthroimidazole) moiety to the electron rich (TPA) molecule to improve the electron mobility and the charge balance in the device structure, which ultimately improve the overall performance of the OLED device efficiency. In the present study, an attempt has been made to functionalize the N_1 position of a phenanthroimidazole moiety with the different functional group (Php-CF_3 and Phm-CF_3) to fine tune the emission towards the blue region. We have designed and synthesized two star shaped fluorophores containing a hole-transporting triphenylamine moiety and an electron-transporting phenanthroimidazole moiety with different functional substitution in the N_1-position of the phenanthroimidazole molecule (Php-CF_3 and Phm-CF_3). Both the fluorophores are structurally characterized by spectroscopic methods. Electrochemical analysis has also been carried out in order to obtain the HOMO-LUMO levels. The fluorophores structures were optimized by using density functional theory (DFT) calculation and the locations of the energy levels (singlet and triplet) are calculated by using time-dependent DFT (TD-DFT) method. Multilayer OLEDs have been fabricated with these fluorophores as emissive materials.

2. Experimental section

2.1. General information and measurements

All the reactions were performed under nitrogen atmosphere. Solvents were carefully dried and distilled from appropriate drying agents prior to use. Commercially available reagents (Sigma Aldrich) were used without further purification unless otherwise stated. All the reactions were monitored by thin-layer chromatography (TLC) with silica gel 60 F_{254} Aluminium plates (Merck). Column chromatography was carried out using silica gel (Sigma-Aldrich). ^{1}H NMR and ^{13}C NMR spectra were recorded using an AV 400 Avance-III 400 MHz FT-NMR Spectrometer (Bruker Biospin International, Switzerland) with tetramethylsilane (TMS) as a standard reference. Elemental analysis was obtained using Elementary Analysis System, Germany/Vario EL spectrometer.

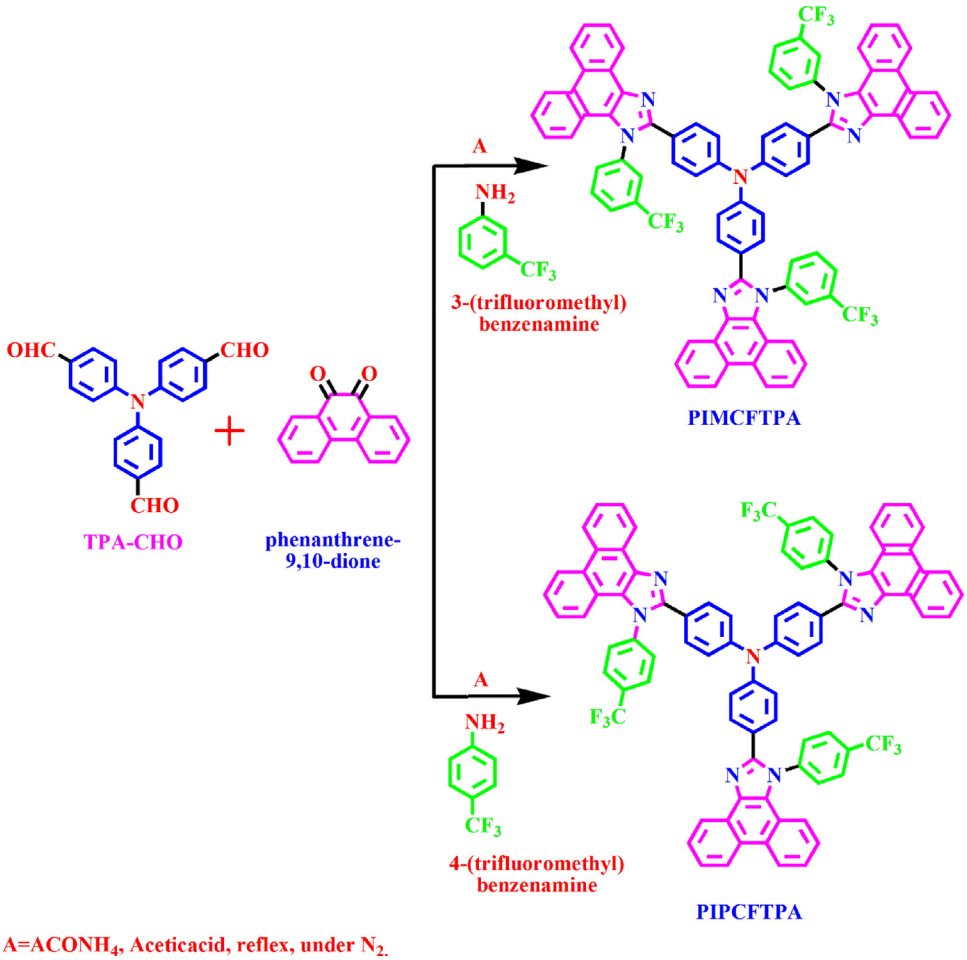

Scheme 1. Synthetic routes for the triphenylamine-phenanthreneimidazole derivatives.

The mass spectra were recorded by LC–MS (Perkin–Elmer, USA/Flexer SQ 300 M). The FTIR spectra were recorded on a Perkin–Elmer RX-I FTIR spectrophotometer. Powder XRD data of the fluorophores were recorded with Cu-Kα1 radiation (Rigaku, ULTIMA IV). DSC-TGA was performed using Netzshe, Germany, STA449C/4/MFC/G. The absorption spectrum of the target compound in solution phase and solid (DRS) were measured by using UV–vis spectrometer (Shimadzu Corporation, Japan/UV-2450 Perkin Elmer, USA/Lamda 25). The photoluminescence emission spectra were recorded by Horiba Jobin Yvon, USA/Fluoromax 4P spectrophotometer. Thin films were prepared by a spin coating method using a spin NXG P1A instrument and measured the PL by spectrofluorimetry. The PL quantum yield (PLQY) of the fluorophores in the form of, a thin film and solid were measured with Edinburgh spectrofluorometer FS5. The life time of the fluorophores was measured at 298 K with Edinburgh Instruments FLS 980 and a pulsed xenon lamp was as the excitation source. The electrochemical properties of the target compound were performed by Cyclic Voltammetry (CV), in DCM. For solution process, CV analysis was done by using working, auxiliary (counter) and reference electrodes. The corresponding electrodes are a glass-carbon disk, Pt wire, and Ag/AgCl wire respectively. DCM containing 0.1 M Bu_4NClO_4 was used as reference electrolyte. The optimize structures and HOMO-LUMO energy levels were calculated by using DFT calculation with B3LYP/6-31G (d, p) basis set.

2.2. Synthesis

The tris(4-formyl phenyl)amine (TPA-CHO) intermediates were synthesized according to the literature with modified procedures (SI1 in Supplementary information) [52]. The target PIPCFTPA and PIMCFTPA fluorophores were synthesized by condensation between 9, 10-phenanthrenequinone, substituted amine and TPA-CHO in the presence of ammonium acetate and acetic acid. The synthetic strategy to obtain the target fluorophores is illustrated in Scheme 1.

2.3. General procedure for the synthesis of the triphenylamine-phenanthreneimidazole derivatives

Amine (0.51 g, 3.1eq) was added to a stirred solution of TPA-CHO (0.3 g, 1eq) in glacial acetic acid (20 ml) at room temperature (RT). To this reaction mixture, subsequently ammonium acetate (2.8 g, 40 eq) and 9, 10-phenanthrenequinone (0.66 g, 3.1 eq) were added. The resulting mixture was stirred for 12 h at 110 °C. The reaction was monitored by thin layer chromatography for the completion of the reaction. After cooling, the reaction mixture was poured into minimum amount of cold distilled water and then ammonium hydroxide solution was added. The formed solid was filtered and dissolved in dichloromethane. This was followed by drying with anhydrous sodium sulphate and the solvent was evaporated to get crude compound. The resultant compound was purified with column chromatography by using silica gel (100–200 mesh) and eluent methanol in dichloromethane (DCM) (1:9). The solvent was evaporated and dissolved in minimum amount of THF solution. To this solution, excess of hexane solvent was added to form the solid. After the solid was settled, the solvent was decanted.

2.4. tris(4-(1-(3-(trifluoromethyl)phenyl)-1H-phenanthro[9,10-d] imidazol-2-l)phenyl) amine (PIMCFTPA)

Yield: 60%. ^{1}H NMR (400 MHz, $CDCl_3$, TMS, δ ppm) 8.87 (d, J = 2 Hz, 3H), 8.81 (d, J = 8.4 Hz, 3H), 8.73 (d, J = 8.4 Hz, 3H). 7.95 (d, J = 0.4 Hz, 3H), 7.82-7.67 (m, 15H), 7.57-7.53 (m, 3H), 7.38-729 (m, 9H), 7.17 (d, J = 8 Hz, 3H). 6.96 (d, J = 8.4 Hz, 6H). ^{13}C NMR (100 MHz, $CDCl_3$, TMS, δ ppm) 150.09, 146.79, 138.89, 137.20, 132.11, 130.30, 129.99, 128.86, 127.86, 127.15, 126.92, 126.49, 126.06, 125.94, 125.72, 125.37, 124.61, 123.85, 123.36, 122.65, 122.33, 122.12, 119.98, 30.42. ^{19}F NMR (400 MHz, $CDCl_3$, TMS, δ ppm) −62.69 (s, 3F). IR (KBr, ν/cm-1): 3430, 3060, 1601, 1475, 1324, 1173, 1132, 1069, 857, 755. EI-MS: m/z = 1327.00 $[M+H]^+$. CHNS Analysis: Anal. Calc. for $C_{84}H_{48}F_9N_7$: C, 76.07; H, 3.65; N, 7.39; Found: C, 76.57; H, 3.80; N, 7.51%.

2.5. tris(4-(1-(4-(trifluoromethyl)phenyl)-1H-phenanthro[9,10-d] imidazol-2-l)phenyl)amine (PIPCFTPA)

Yield: 69%. ^{1}H NMR (400 MHz, $CDCl_3$, TMS, δ ppm) 8.87 (d, J = 2 Hz, 3H), 8.79 (d, J = 8.4 Hz, 3H), 8.72 (d, J = 8.4 Hz, 3H). 7.92 (d, J = 8.0 Hz, 6H), 7.79-7.67 (m, 12H), 7.56-7.52 (m, 3H), 7.49-7.39 (m, 3H), 7.33-7.28 (m, 3H), 7.11-7.04 (m, 6H), 6.99-6.95 (m, 6H). ^{13}C NMR (100 MHz, $CDCl_3$, TMS, δ ppm) 149.90, 146.73, 141.58, 137.18, 129.90, 129. 31, 128.84, 127.85, 127.38, 126.93, 126.78, 126.46, 125.98, 125.39, 124.62, 124.51, 123.82, 123.37, 122.63, 122.31, 122.11, 119.97, 115.74, 30.42. ^{19}F NMR (400 MHz, $CDCl_3$, TMS, δ ppm) −62.38 (s, 3F). IR (KBr, ν/cm-1): 3430, 3060, 1601, 1475, 1330, 1177, 1134, 838, 755. EI-MS: m/z = 1326.99 $[M + H]^+$. CHNS Analysis: Anal. Calc. for $C_{84}H_{48}F_9N_7$: 76.07; H, 3.65; N, 7.39; Found: C, 76.26; H, 3.75; N, 7.49%.

3. Results and discussion

3.1. Characterization of the fluorophores

The synthetic strategy to obtain the target fluorophores is illustrated in Scheme 1. The compounds are characterized by nuclear magnetic resonance spectroscopy (^{1}H and ^{13}C NMR), Mass spectrometry, elemental analysis, and Fourier transform infrared spectroscopy (FTIR). FTIR Spectroscopy results are given in Supplementary information (SI3)

3.2. Powder X-ray diffraction (XRD) studies

Powder X-ray Diffraction studies were performed to evaluate the crystalline or amorphous nature of the synthesized fluorophores (Fig. 1). XRD pattern of the fluorophores was recorded in the 2θ range between 10 and 60°. The diffraction peaks of both the fluorophores show amorphous phase without the appearance of any peak. General, amorphous fluorophores are highly required to

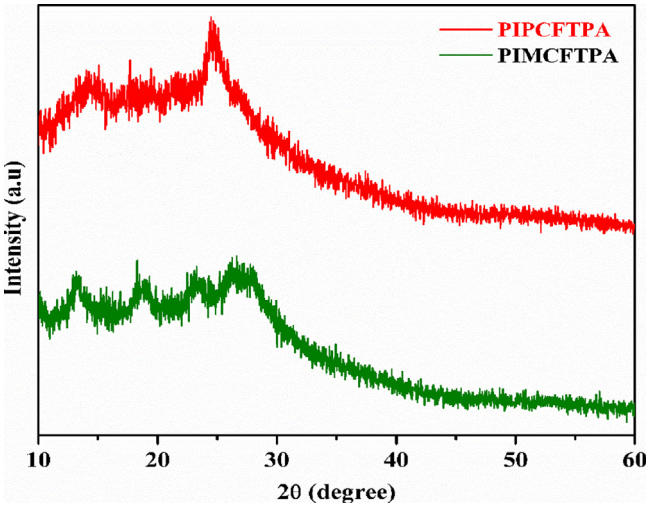

Fig. 1. Powder X-ray diffraction patterns of PIPCFTPA and PIMCFTPA fluorophores.

fabricate the OLEDs, where the fluorophores should not be crystalline in the device working conditions. The currently synthesized fluorophores showed potent to be used as emissive materials for OLED device.

3.3. Thermal properties

The thermal behavior of PIMCFTPA and PIPCFTPA were investigated by thermogravimetric analysis (TGA) and differential scanning calorimetry (DSC) under nitrogen atmosphere. DSC-TGA measurements were carried out from 0 to 700 °C at a scanning rate of 10 °C/min. DSC-TGA curves of synthesized fluorophores were depicted in Fig. 2. The TGA curves reveal that the degradation temperature (T_d) of 10% weight loss of PIMCFTPA and PIPCFTPA is 275 °C and 377 °C, respectively. Fig. 2B shows the glass transition temperatures of the synthesised compounds and has a hump between 210 and 240 °C. These humps are indicating that the phase change is occurring with respect to temperature. The exact values of the glass transition temperature of the compounds were determined by drawing a tangent at the hump (Fig. 2B), and their glass-transition temperatures (T_g) are 235 °C and 240 °C, respectively. The significant enhancement of T_g can be attributed to the introduction of two phenanthroimidazole moieties, which would reduce the possibility of phase separation upon heating and may prolong the lifetime of the devices. These DSC-TGA results suggest that the currently investigated fluorophores possess high thermal decomposition temperatures which is one of the essential requirements for OLEDs.

3.4. Photophysical properties

The absorption and fluorescence spectra of the fluorophores in chloroform ($CHCl_3$) solution (10^{-5} mol L^{-1}), (Fig. 3A) as well as in film state on quartz substrates (Fig. 3B) were studied to investigate the photophysical properties. Key photophysical parameters of the two emitters are listed in Table 1. For both the fluorophores, the absorption spectra exhibit no distinct differences and both exhibit two peaks at around 265 nm and 376 nm in $CHCl_3$ solution. The absorption peaks at about 265 nm for both the fluorophores are attributed to the $\pi-\pi^*$ transition of benzene ring [53], while the absorption bands at 376 nm arise from the $\pi-\pi^*$ transition from the triphenylamine and the phenanthroimidazole moiety. The optical bandgap of the fluorophores calculated from the solid-state (DRS) absorption spectra (Fig. 3D) with the help of Kubelka-Munk function [54] are 2.82 eV (PIMCFTTPA) and 2.71 eV (PIPCFTPA). The photoluminescence spectra for PIMCFTPA and PIPCFTTPA in $CHCl_3$ show a sharp emission peak at approximately 440 nm. The absorption spectra of these films were found to be broad and red-shifted as compared with a solution (303, 381 nm). The photoluminescence spectra of the fluorophores in a neat film peaked at 455 nm and 460 nm respectively, which are red shifted (Table 1) by 15–20 nm from their solutions. Similar observations were also observed for solid PL spectra (Fig. 3B). The observed redshifts can be explained by their relative strong $\pi-\pi$ stacking interactions [55]. The CIE chromaticity coordinates for fluorophores shown Fig. 3C.

Fluorescence quantum yield (Φ_f) is an important parameter for the quantitative characterization of fluorophores. The Φ_f of the fluorophores was calculated using 9,10-diphenyl anthracene as a standard (Φ_{ref} = 0.90 in cyclohexane) according to equation [56],

$$\Phi_f = \Phi_{ref}\left(\frac{S_{sample}}{S_{ref}}\right)\left(\frac{A_{ref}}{A_{sample}}\right)\left(\frac{n^2_{sample}}{n^2_{ref}}\right) \quad (1)$$

Where S_{sample}, A_{sample}, $n_{sampleand}$ S_{ref}, A_{ref}, n_{ref} represent the integrated emission band area, the absorbance at the exited wavelength, and the refractive index of the solvent, respectively for the standard reference and the sample. The quantum yields of the fluorophores are 0.31 (PIPCFTPA) and 0.26 (PIMCFTPA).

The absolute quantum yield (QY) of the fluorophores was calculated using an integrating sphere for both thin films and solid samples. The absolute quantum yields (Φ) (integration sphere) of the fluorophores calculated by the following Eq. (2) [57].

$$\Phi = \frac{L_0(\lambda) - L_i(\lambda)}{L_0(\lambda)} \quad (2)$$

$$\eta = \frac{E_i(\lambda) - (1-\Phi)E_0(\lambda)}{E_0(\lambda)\Phi}$$

Where, $L_0(\lambda)$ is the integrated excitation profile (sample is directly excited by the incident beam) and $L_i(\lambda)$ are the integrated excitation profile attained from the empty integrated sphere. $E_0(\lambda)$ is the integrated luminescence of powder caused by direct excitation and Ei(λ) is indirect illumination from the sphere, respectively. The calculated QY of the fluorophores, PIPCFTPA and PIMCFTPA are 14.81 and 16.36% in thin film, respectively. In the case of solid fluorophores showed is 24 and 25.4% for PIPCFTPA and PIMCFTPA, respectively. The measured QY results are tabulated in

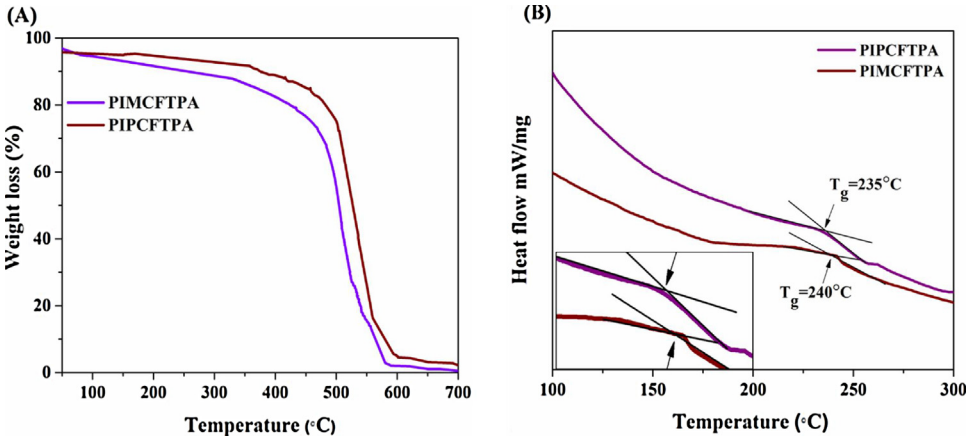

Fig. 2. (A) TGA and (B) DSC curves of PIMCFTPA and PIPCFTTPA.

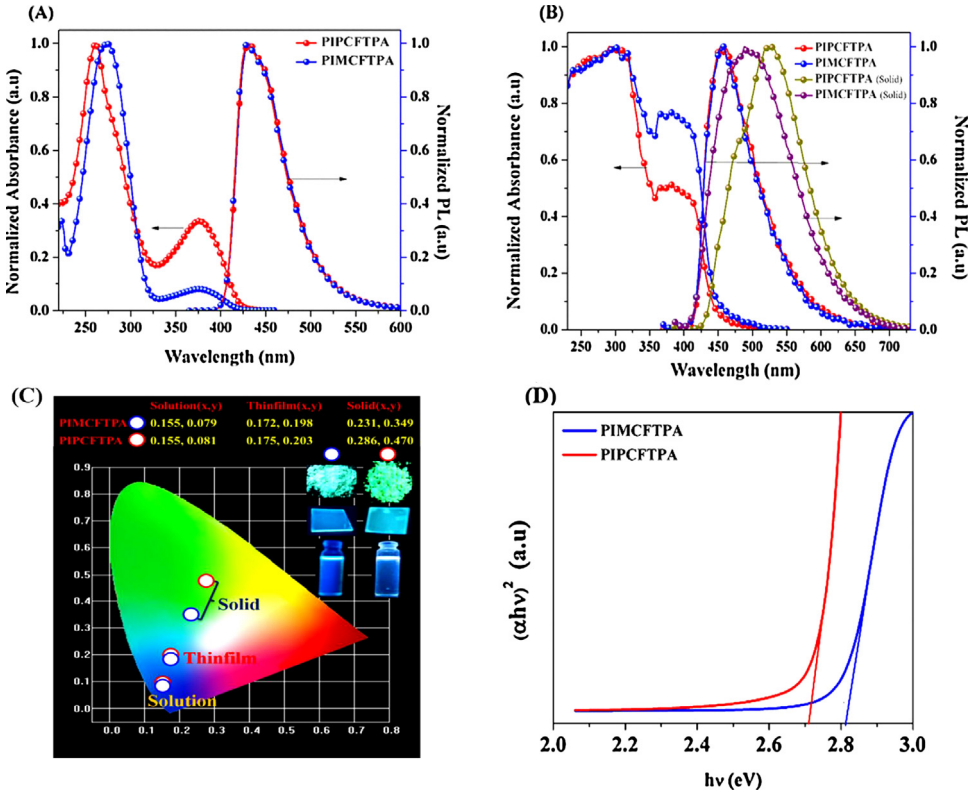

Fig. 3. (A) UV absorption and PL spectra of PIPCFTPA and PIMCFTPA in $CHCl_3$ solution, (B) in the film and solid state, (C) The CIE chromaticity coordinates for fluorophores and (D) optical bandgap of the fluorophores calculated from the solid-state diffuse reflectance spectra.

Table 1
Key photophysical properties of PIPCFTPA and PIMCFTPA.

Compounds	T_g[a]/T_d[a]°C	Solution		Φ_f[b]	Absolute quantum yield		Film		Solid PL (nm)	λ_{abs} (nm) (calculated) (*f*)[c]
		Abs (nm)	PL (nm)		Film (%)	Solid (%)	Abs (nm)	PL (nm)		
PIPCFTPA	220/377	265, 376	441	0.31	14.81	24	303, 381	460	520	414 (0.828)
PIMCFTPA	190/275	273, 376	432	0.26	16.36	25.4	303, 381	455	493	404 (0.879)

[a] Glass transition temperature, thermal decomposition temperature.
[b] Fluorescent quantum yield in solution measured with respect to 9,10-diphenyl anthracene.
[c] Calculated at B3LYP/6-31G (d,p) basis set, in the gas phase, *f* = Oscillator Strength.

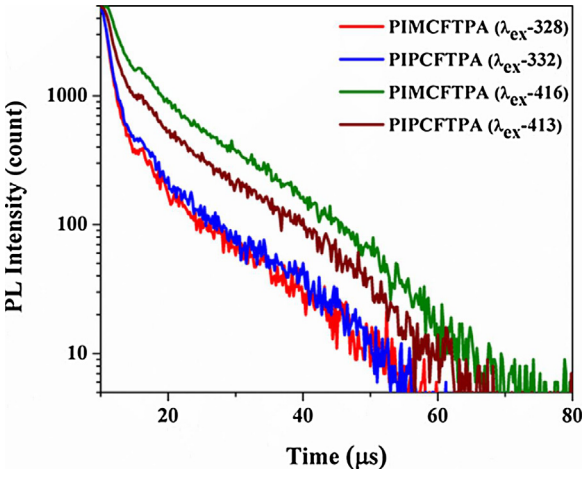

Fig. 4. Fluorescence lifetime decay curves.

Table 1. The measured QY digital images are shown in Figs. S12 and S13 in Supplementary information.

3.5. Fluorescence lifetime

The fluorescence lifetime of fluorophores PIPCFTPA and PIMCFTPA at 10^{-4} M concentrations were measured using time-correlated single photon counting technique and the decays are shown in Fig. 4. The decays were fitted mono-exponential function given by the equation $(t) = I_0 + A_1 \exp(-t/\tau)$, where $I_0 = 0$ is the offset value, A_1 is the scalar quantity obtained from the curve fitting, t is the time in μs and τ is the decay time value for the exponential component and the fluorescence lifetime of fluorophores PIPCFTPA and PIMCFTPA were found to be between 1 and 6 μs (Table 2) [58–60].

3.6. Solvatochromism study

Solvatochromism study was also carried out for PIPCFTPA and PIMCFTPA. Interaction of solvent-dependent emission spectra appear simple but it is complicating due to the fluorophores'

Table 2
Fluorescence lifetimes of PIPCFTPA and PIMCFTPA.

Compounds	Excitation wavelength (nm)	Emission wavelength (nm)	Life time (τ_1) in μs
PIPCFTPA	328	441	1.96
	416	441	3.40
PIMCFTPA	332	432	1.70
	413	432	6.04

multiple interactions with their local environment, which results in spectral (either red or blue) shifts. The emission of the fluorophores was accomplished under different solvents: acetonitrile (ACN) dimethylformamide (DMF), dichloromethane (DCM), chloroform ($CHCl_3$), tetrahydrofuran (THF), and toluene, and their Stokes shifts were measured. The solvatochromism of fluorophores was interpreted in terms of Lippert-Mataga equation. It defines the Stokes shift in terms of the changes that occur in the dipole moment during excitation. By increasing the polarity of the solvent, the red (bathochromic) shift was observed, which are showed in Fig. 5 (PIPCFTPA) and Fig. 6 (PIMCFTPA). The Eqs. ((3) and (4)) of Lippert–Mataga describes the Stokes shift $\Delta\overline{\nu}$ (expressed in wavenumbers) as a function of the change of the dipole moment ($\Delta\mu_{ge} = \mu_e - \mu_g$) of the fluorophore. Solvents with dissimilar dielectric constants (ε) and refractive indices (n) are used in the Eq. (4) and the plot was drawn Stokes shift ($\Delta\overline{\nu}$) as a function of Δf [61].

$$\Delta\overline{\nu} = \frac{2\Delta f}{4\pi\varepsilon_0 hca^3}(\mu_e - \mu_g) + \text{Constant} \quad (3)$$

$$f(\varepsilon) = \frac{f(\varepsilon - 1)}{f(2\varepsilon + 1)} \text{and} f(n^2) = \frac{(n^2 - 1)}{(2n^2 + 1)} \quad (4)$$

where, $\Delta\overline{\nu} = \Delta\overline{\nu}_{abs} - \Delta\overline{\nu}_{em}$ is the solvatochromic shift (in cm^{-1}) between the maxima of absorption and fluorescence emission [$\Delta\overline{\nu}_{abs} = 1/\lambda_{abs}(max)$, $\Delta\overline{\nu}_{em} = 1/\lambda_{em}(max)$], h is Planck's constant, c is the velocity of light, ε_0 is the permittivity of vacuum (signifies the radius of the cavity in which the solute resides); μ_e and μ_g are dipole moments in the excited and ground states. The solvatochromism data is tabulated in Table S2 (Supplementary information). It was also verified using Lippert–Mataga equation (Fig. S14 in Supplementary information). Fig. S14 represents the Lippert–Mataga plot for PIPCFTPA and PIMCFTPA in different solvents and the corresponding data is listed in Table S2. Fig. S14 (A) indicates the linear relationship [correlation coefficient r = 0.460, slope = $(0.588) \times 10^3\ cm^{-1}$, intercept = $(7.052) \times 10^3\ cm^{-1}$] of the Stokes shift, $\Delta\overline{\nu}$ verses Δf for different solvents of PIPCFTPA. Similarly, Fig. S14 (B) indicates the linear relationship [correlation coefficient r = 0.499, slope = $(3.862) \times 10^3\ cm^{-1}$, intercept = $(0.340) \times 10^3\ cm^{-1}$] of the Stokes shift, $\Delta\overline{\nu}$ verses Δf for PIMCFTPA.

3.7. Theoretical calculations

To gain insight into the electronic structures of the fluorophores, density functional theory (DFT) calculation was performed at the B3LYP/6-31G (d,p) basis set. The DFT-calculated optimized geometries of these fluorophores (Fig. 7) in gas phase show slightly twisted conformations [62]. In PIMCFTPA, dihedral angles between Phenanthroimidazole and triphenylamine plane (28.41°) is slightly more than PIPCFTPA (27.03°), due to a twisted substituent on the 1-imidazole position. As shown in Fig. 7. The electron density contours of the lowest unoccupied (LUMO) and the highest occupied molecular orbitals (HOMO) for fluorophores are presented. The HOMO levels mainly populate on the triphenylamine (TPA) for both the fluorophores, whereas, the LUMO were exclusively located on phenanthroimidazole moiety (Table 4). The calculated HOMO/LUMO values of the fluorophores are -4.93/-1.43 eV (PIMCFTPA) and −4.94/-1.52 eV (PIPCFTPA), respectively. The predicted HOMO–LUMO energy gaps of 3.50 (PIMCFTPA) and 3.42 eV (PIPCFTPA) are in good alignment with the experimental results (Table 5). The singlet and triplet energy levels were calculated by using time-dependent density functional theory (TD-DFT) analysis and are included in Table 3. The most intense peak in PIPCFTPA is at 414 nm with oscillator strength $f = 0.828$. In PIMCFTPA, it is at 404 nm with $f = 0.879$ are shown Fig. S15 in the Supplementary information. The substituent at N_1 position showed less impact on the absorption phenomenon in these fluorophores. In addition, atom coordinates and absolute energies of PIMCFTPA and PIPCFTPA were given in Supplementary information. (SI7 in Supplementary information)

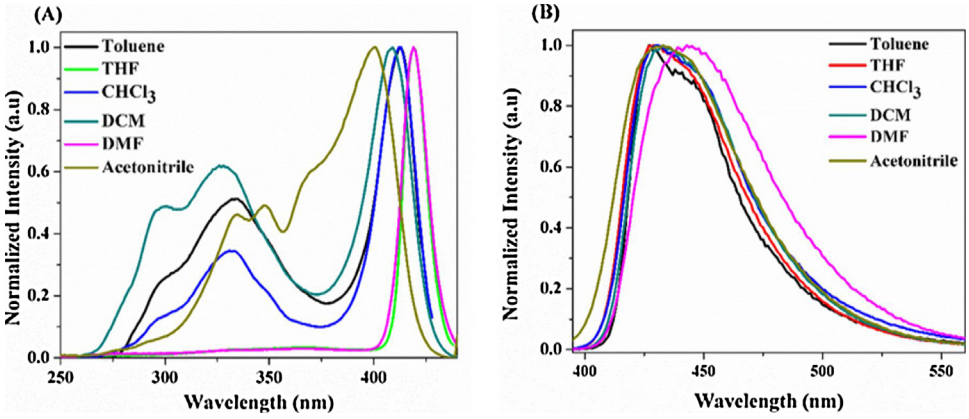

Fig. 5. (A) Excitation and (B) emission spectra of PIPCFTPA in different solvents.

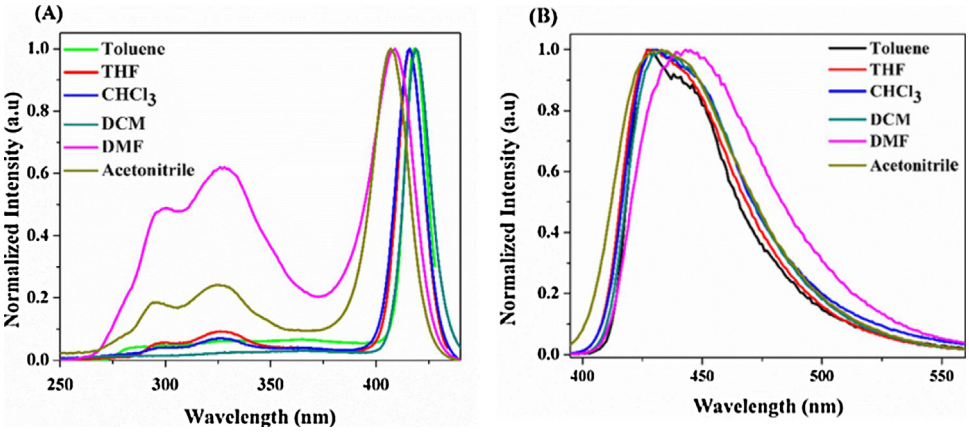

Fig. 6. (A) Excitation and (B) emission spectra of PIMCFTPA in different solvents.

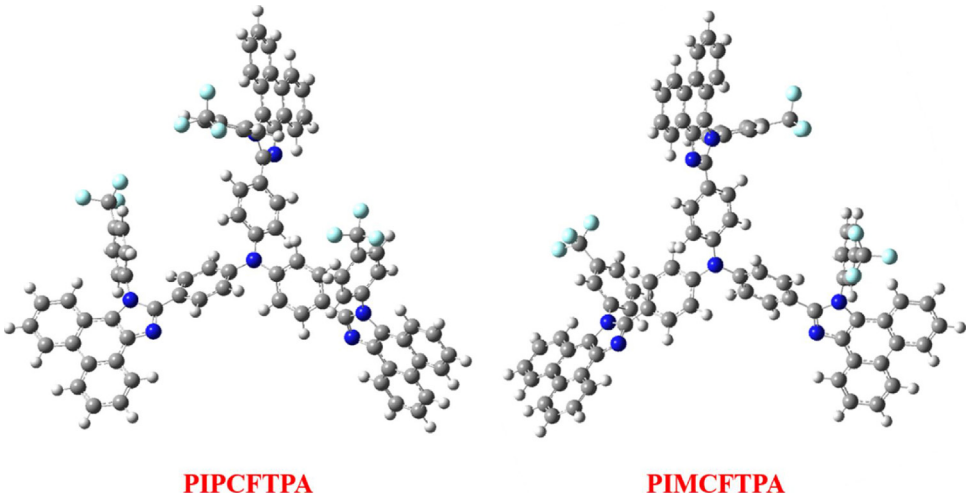

Fig. 7. Optimized structures of PIPCFTPA and PIMCFTPA.

Table 3
Calculated Frontier Molecular Energy Levels.

Molecule	HOMO (eV)	LUMO (eV)	E_g (eV)	S1 (gas) (eV)	T1 (gas) (eV)
PIPCFTPA	−4.94	−1.52	3.42	2.98	2.48
PIMCFTPA	−4.93	−1.43	3.50	3.05	2.48

3.8. Electrochemical properties

The electrochemical properties of the fluorophores were investigated by cyclic voltammetry (CV) using 0.1 M Tetrabutylammonium perchlorate (Bu_4NClO_4) as a supporting electrolyte in acetonitrile solution at a scan rate of 100 mV s^{-1}. The cyclic voltammograms are shown in Fig. 8 and the corresponding electrochemical data is summarized in Table 5. Fig. 8 shows that both the fluorophores have distinct oxidation and reduction behaviors. According to the onset potentials, we calculated the highest occupied molecular orbital (HOMO) and the lowest unoccupied molecular orbital (LUMO) energy levels by using the Eqs. (5) and (6) reported by de Leeuw et al. [63]

$$E_{HOMO} = -(E_{ox}^{onset} + 4.4)eV \quad (4)$$

$$E_{LUMO} = -(E_{red}^{onset} + 4.4)eV \quad (5)$$

The HOMO/LUMO energy levels of the fluorophores are −5.62/−3.34 eV (PIMCFTPA) and −5.62/−3.36 eV (PIMCFTPA), respectively with energy bandgap of 2.28 (PIMCFTPA) and 2.26 eV (PIPCFTPA). The HOMO-LUMO results of both the fluorophores suggest that they can be used as host materials as their HOMO/LUMO energy levels are similar to commercially available host materials like CBP [64]. The comparison of HOMO-LUMO energy gap of both the fluorophores is shown in Fig. 9. It clearly indicates that the band gaps calculated using both optical and electrochemical analysis almost match.

3.9. Electroluminescence studies

As the final part of the investigation, OLED devices with TPA derivatives (PIPCFTPA and PIMCFTPA) as emissive materials, were fabricated with the device configuration: ITO (120 nm)/F_4TCNQ (4 nm)/α-NPD (40 nm)/TPA derivatives (30 nm)/BCP (6 nm)/LiF (0.5 nm)/Al (150 nm). For the convenience of discussion, the two OLED devices were named device A and device B for the OLEDs based on PIPCFTPA and PIMCFTPA, respectively. The schematic of the OLED structure and related HOMO/LUMO energy levels of the derivatives along with other materials used in the electroluminescent devices are illustrated in Fig. 10. Here ITO (indium-tin oxide) served as a transparent anode. F_4TCNQ (2,3,5,6-Tetrafluoro-7,7,8,8-tetracyano quinodimethane) was chosen as hole-injection layer (HIL) as it efficiently injects holes from the ITO anode to hole-

Table 4
Electron Density Contours of frontier molecular orbitals (FMO).

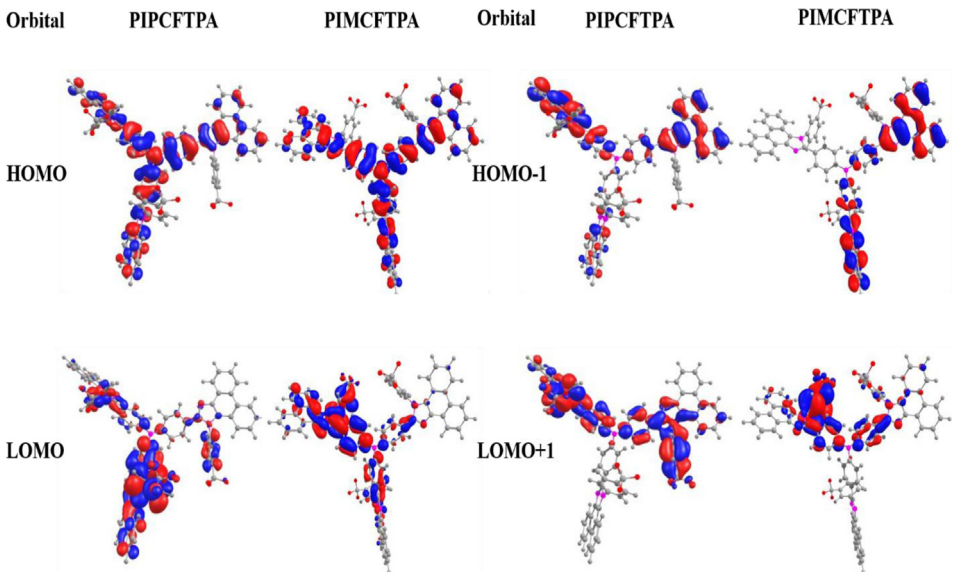

Table 5
Electrochemical properties of PIPCFTPA and PIMCFTPA.

Compounds	E_{ox}[a] (V)	E_{red}[a] (V)	HOMO (eV)	LUMO (eV)	E_g[b] (eV)	E_g[c] (eV)	E_g[d] (eV)
PIMCFTPA	1.22	−1.06	−5.62	−3.34	2.82	2.28	3.50
PIPCFTPA	1.22	−1.04	−5.62	−3.36	2.71	2.26	3.42

[a] The onset potential.
[b] Optical energy bandgap estimated from the solid-state DRS spectra.
[c] Electrochemical bandgap determined from cyclic voltammetry.
[d] Theoretical bandgap.

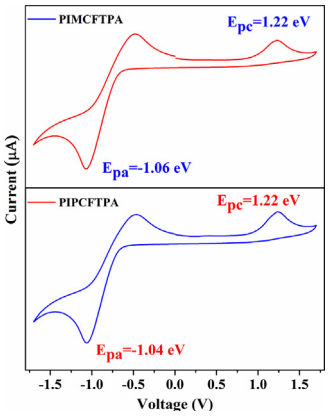

Fig. 8. Cyclic voltammograms of PIPCFTPA and PIMCFTPA.

transport-layer. An optimized thickness of F_4TCNQ was used for better hole injection as reported earlier. [65], α-NPD (4,4′-bis[*N*-(1-naphthyl)-*N*-phenyl-L-amino]-biphenyl) was chosen as the hole-transporting layer (HTL) because of its high HOMO energy (similar to the fluorophores); in addition, considering the energy levels (shown in Fig. 10) of materials used in the OLEDs, α-NPD with a higher LUMO level also plays a role of an effective electron-blocking material. By using BCP (bathocuproine) as hole-blocking layer (HBL), the reductant holes are confined in the emitting layer which didn't recombine with the electrons in the emitting zone [66]. LiF (lithium fluoride) and Al (aluminum) were used as the electron-injecting layer (EIL) and cathode, respectively.

Fig. 11(a) depicts the steady-state electroluminescence (EL) spectra of the devices at the driving voltages of 10 V for device A and device B with bluish green light emission with peaks centred at 511 (shoulder peak: 436) and 505 (shoulder peak: 442) nm, respectively with full-width at half maxima (FWHM) of 72 and 60 nm. The EL peaks show bathochromic shifts with respect to the thin film PL peaks. This bathochromic shift of EL peaks with respect to PL can be due to the result of exciplexes formation [55,67,68]. Furthermore, as shown in Fig. 11(b), the EL spectra of both the devices showed the same profile without any effect on the shape and EL spectra peak under various driving voltages. Hence, both the devices exhibited excellent spectral stability over a wide range of operating voltages. The Commission Internationale de l'Eclairage (CIE) chromaticity coordinates of the derivatives as EL materials are determined using the EL spectra of the devices at 10 V. The chromaticity diagram is shown in Fig. 11(c) and the CIE coordinates are tabulated in Table 6. Fig. 11(d) displays the current density-voltage-luminance (J-V-L) characteristics of the fabricated OLEDs. The characteristics of the current density as a function of applied voltage reveal good diode behavior. Both the devices

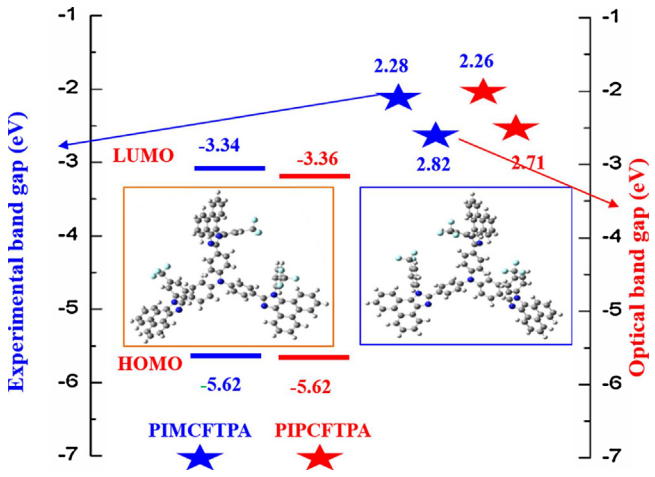

Fig. 9. HOMO – LUMO energy gap diagram of PIPCFTPA and PIMCFTPA.

exhibited good current density demonstrating good charge transport capability. The devices A and B turns on at very low bias voltages (corresponding to 1 cd/m^2) of 2.98 and 2.83 V, respectively indicating low charge injection barriers. The devices showed maximum luminance (L_{max}) of 1261 cd/m^2 (device A) and 2132 cd/m^2 (device B) at 10 V. The current, output power and external quantum efficiencies for both the devices along with other parameters of the devices are summarized in Table 6. In assessing the performance of the two devices, device B (based on PIMCFTPA) showed better performance with current efficiency (η_c) of 6.58 cd/A, power efficiency (η_p) of 5.91 lm/W and external quantum efficiency (η_{ext}) of 3.62% corresponding to 100 cd/m^2. The device efficiency versus luminance curves of the devices are shown in Fig. S15 in Supplementary information. As you can see, in the EL spectra of the fluorophores, the PIMCFTPA fluorophore shows blue shift emission in the EL spectra. This can be attributed to the strong electron withdrawing (CF_3) linked at the m-position of N_1-substitution which restricts the free conjugation more than p-position N_1-substitution, thus leads to an increase in the band gap of the PIMCFTPA fluorophore and in term, causing blue shift in the EL spectra. The results suggest that though the derivatives have comparatively moderate PL quantum efficiency, the charge carrier balance is significantly strong (injection barrier for holes and electrons), which results in high EQE (EQE = $\gamma\ \chi\ \eta_{pl}\ \eta_{oc}$, where γ is the recombination efficiency of injected holes and electrons, χ is the fraction of excitons that can potentially radiatively decay due to restriction of multiplicity, η_{PL} is the PL yield and η_{oc} is the out-coupling efficiency) [69]. It appears that the devices possess balanced charge transport for holes and electrons. This may arise from the relatively low barrier for the hole and electron injection from the HTL and ETL, respectively into the active layers. To the best of our knowledge, these values are among the best comparing the reported non-doped OLEDs [40,45,70,71]. It is noteworthy that, during the measurements, both the devices did not damage at higher applied electrical voltages, perhaps due to the high thermal stabilities of the fluorophores. This observation offers the potential use of the fluorophores in OLED applications.

4. Conclusion

In summary, we have successfully designed and synthesized star shaped electroluminescent phenanthroimidazole-based fluorophores (donor–π-acceptor) by integrating the triphenylamine core (electron-donating moiety) to the phenanthroimidazole (electron-accepting moiety) with different linkers in N_1-position (Php-CF3 and Phm-CF3). The fluorophores show good thermal stability as well as high glass transition temperatures. The electrochemical analysis reveals that both the fluorophores have distinct oxidation and reduction behaviors. Device with PIMCFTPA emitter exhibits high efficiencies (6.58 cd/A, 5.91 lm/W, and 3.62%) with low turn-on voltage of 2.83 V than that of PIPCFTPA (5.99 cd/A, 4.53 lm/W, 3.49%). Both the fluorophores show bluish green emission with CIE coordinates of x = 0.223, y = 0.405 (PIMCFTPA) and x = 0.281, y = 0.415 (PIPCFTPA), respectively. These results demonstrate that these derivatives are promising candidates and could play an important role in the development of OLEDs.

4.1. Fabrication and characterization of OLEDs

To fabricate OLED devices, pre-patterned ITO (Kintec, Hong Kong) coated glass substrates, with a sheet resistance of 15 Ω/□ and ITO thickness of 120 nm, were used as the anode. Prior to the deposition of organic materials, ITO substrates were cleaned and UV-Ozone treated according to the procedure reported earlier [7]. All organic materials and cathode layers were deposited by thermal evaporation at a base pressure of 5×10^{-6} Torr. On the ITO substrate, the HIL, HTL, emitting layer, HBL, EIL, and cathode were deposited sequentially without breaking the vacuum. F_4TCNQ

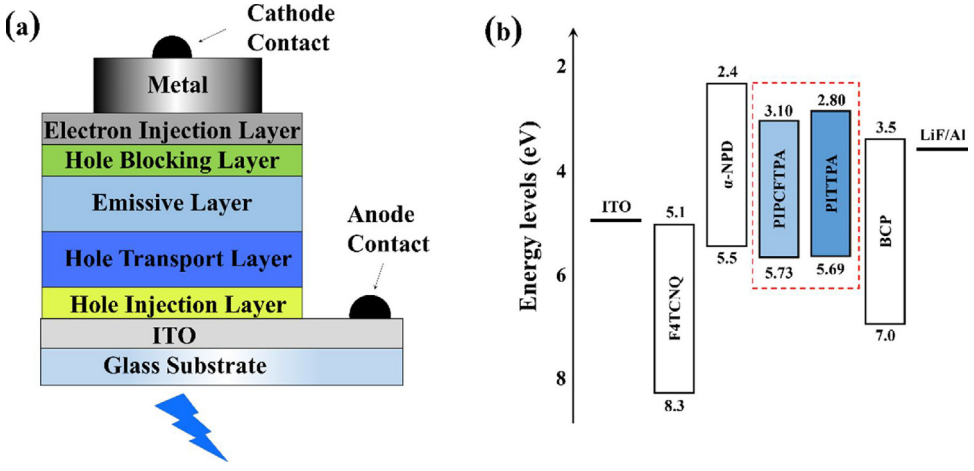

Fig. 10. (a) Schematic diagram of the OLED structure and (b) Energy-level diagram of the materials used in this study.

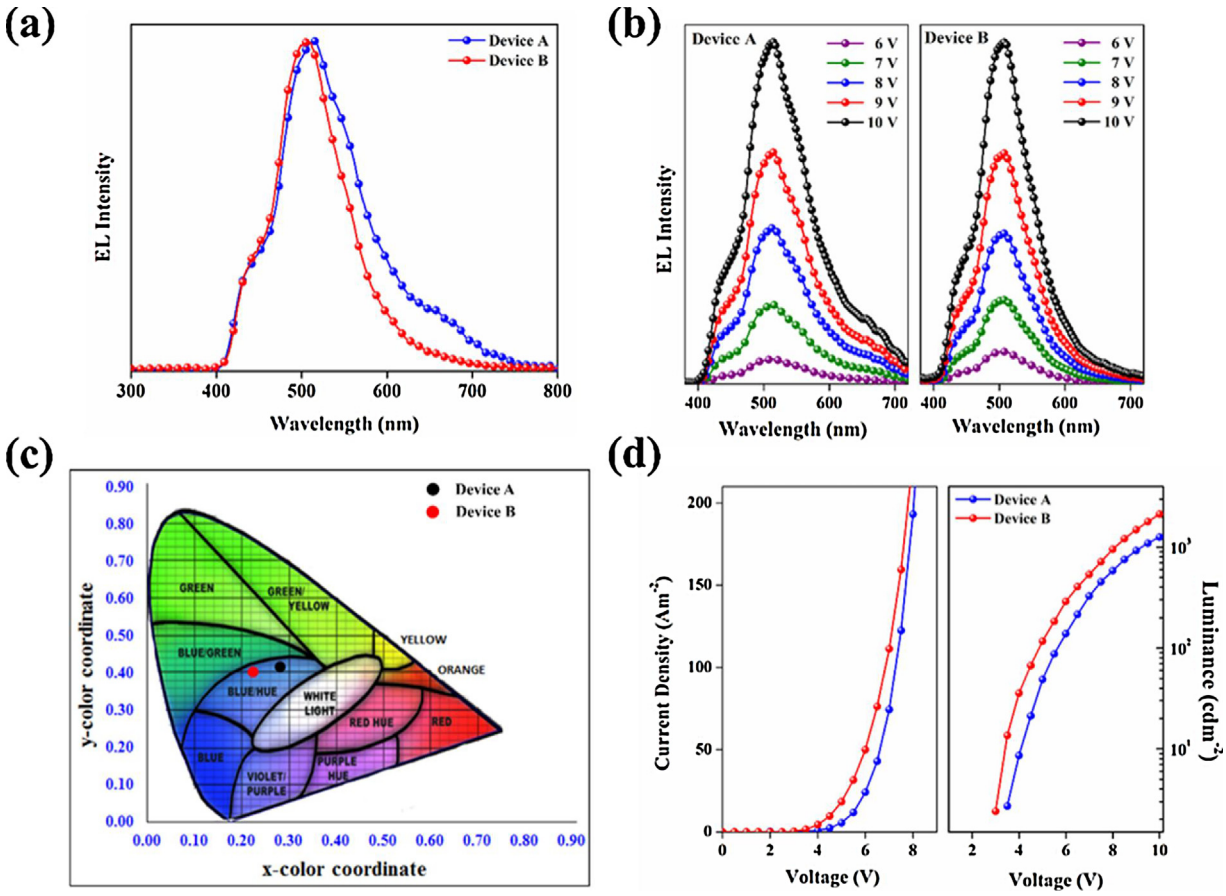

Fig. 11. (a) EL spectra, (b) EL spectra at different applied voltages, (c) Chromaticity diagram and (d) Current density–voltage–luminance (J–V–L) characteristics of the OLEDs with TPA as emissive materials.

Table 6
Electroluminescent performance data of OLEDs using TPA derivatives as emissive materials.

Device[a]	V_{onset} (V)[b]	L_{max} (cd m^{-2})[c]	η_c (cd A^{-1})[d]	η_p (lm W^{-1})[d]	η_{ext} (%)[d]	λ_{em} (FWHM) (nm)[e]	CIE $_{(x,y)}$[f]
PIPCFTPA	2.98	1261	5.99	4.53	3.49	436, 511 (72)	(0.281, 0.415)
PIMCFTPA	2.83	2132	6.58	5.91	3.62	442, 505 (60)	(0.223, 0.405)

[a] Device Configuration: ITO (120 nm)/F_4TCNQ (4 nm)/α-NPD (40 nm)/TPA (30 nm)/BCP (6 nm)/LiF (0.5 nm)/Al (150 nm).
[b] V_{onset}: turn-on voltage at luminance of 1 cd m^{-2}.
[c] $L_{max:}$ Maximum luminance at 10 V.
[d] η_c: Current, power and external quantum efficiencies measured at 100 cdm^{-2}.
[e] λ_{em}: Emission wavelength maximum. FWHM: full-width half maximum at 10 V.
[f] CIE color coordinates.

(LUMTEC) was used as HIL, α-NPD (LUMTEC) was used as the HTL, BCP (Sigma-Aldrich) was used as HBL, LiF (Sigma-Aldrich) was used as EIL and Al (Alfa Aesar) was used as the cathode. All the organic materials were used as received without further purification. The deposition rate of organic materials was maintained at 0.5 Å s^{-1}, whereas the deposition rates of LiF and Al were 0.1 Å s^{-1} and 6 Å s^{-1} respectively. The deposition rates and thickness of the deposited layers were controlled in situ by a quartz crystal thickness monitor placed near the substrate. The cathode was deposited on the top of the structure through a shadow mask. The light-emitting area was 1.6 mm as defined by the overlap of the cathode and anode. All the electro-optical characteristics/properties of OLEDs such as EL spectra and J-V-L characteristics of the devices were measured using a spectrophotometer (Horiba Jobin Yvon iHR320), a computer-controlled, programmable source-meter (Keithley 2400) and calibrated Si photodiode (SM1PD2A). CIE coordinates were calculated from the EL spectra. Devices were driven under dc conditions. All the measurements were carried out at room temperature under dark and ambient conditions without any encapsulation.

Acknowledgements

T. J. and V. S. acknowledge *INSPIRE, DST. India* (INSPIRE FACULTY AWARD no: IFA12-CH-48 and SERB/2016/002462) for the financial support. H.U. and M.N.S. acknowledge Department of Information Technology (Grant No. 12(3)/2010-PDD), India and NITK, Surathkal for the financial support.

Appendix A. Supplementary data

Supplementary data associated with this article can be found, in the online version, at https://doi.org/10.1016/j.jphotochem.2017.11.001.

References

[1] C.W. Tang, S.A. VanSlyke, Organic electroluminescent diodes, Appl. Phys. Lett. 51 (1987) 913.
[2] S.R. Forrest, The path to ubiquitous and low-cost organic electronic appliances on plastic, Nature 428 (2004) 911.
[3] B.W. D'Andrade, S.R. Forrest, White organic light-emitting devices for solid-state lighting, Adv. Mater. 16 (2004) 1585–1595.
[4] X. Qi, M. Slootsky, S. Forrest, Stacked white organic light emitting devices consisting of separate red, green, and blue elements, Appl. Phys. Lett. 93 (2008) 193306.
[5] N. Chopra, J. Lee, Y. Zheng, S.H. Eom, J. Xue, F. So, High efficiency blue phosphorescent organic light-emitting device, Appl. Phys. Lett. 93 (2008) 143307.
[6] Z. Zhang, Q. Wang, Y. Dai, Y. Liu, L. Wang, D. Ma, High efficiency fluorescent white organic light-emitting diodes with red green and blue separately monochromatic emission layers, Org. Electron. 10 (2009) 491–495.
[7] H. Ulla, M. Raveendra Kiran, B. Garudachari, M.N. Satyanarayan, G. Umesh, A.M. Isloor, Blue emitting halogen-phenoxy substituted 1,8-naphthalimides for potential organic light emitting diode applications, Opt. Mater. 37 (2014) 311–321.
[8] J.H. Lee, S.H. Cheng, S.J. Yoo, H. Shin, J.H. Chang, C.I. Wu, K.T. Wong, J.J. Kim, An exciplex forming host for highly efficient blue organic light emitting diodes with low driving voltage, Adv. Funct. Mater. 25 (2015) 361.
[9] Q. Wang, I.W.H. Oswald, X. Yang, G. Zhou, H. Jia, Q. Qiao, Y. Chen, H.J. Hoshikawa, B.E. Gnade, A non-doped phosphorescent organic light-emitting device with above 31% external quantum efficiency, Adv. Mater. 26 (2014) 8107.
[10] C. Tang, R. Bi, Y. Tao, F. Wang, X. Cao, S. Wang, T. Jiang, C. Zhong, H. Zhang, W. Huang, A versatile efficient one-step approach for carbazole-pyridine hybrid molecules: highly efficient host materials for blue phosphorescent OLEDs, Chem. Commun. 51 (2015) 1650.
[11] W. Grice, D.D.C. Bradley, M.T. Bernius, M. Inbasekaran, W.W. Wu, E.P. Woo, High brightness and efficiency blue light-emitting polymer diodes, Appl. Phys. Lett 73 (1998) 629.
[12] M.A. Baldo, D.F. O'Brien, Y. You, A. Shoustikov, S. Sibley, M.E. Thompson, S.R. Forrest, Highly efficient phosphorescent emission from organic electroluminescent devices, Nature 395 (1998) 151.
[13] M.A. Baldo, M.E. Thompson, S.R. Forrest, High-efficiency fluorescent organic light-emitting devices using a phosphorescent sensitizer, Nature 403 (2000) 750.
[14] H. Nakanotani, T. Higuchi, T. Furukawa, K. Masui, K. Morimoto, M. Numata, H. Tanaka, Y. Sagara, T. Yasuda, C. Adachi, High-efficiency organic light-emitting diodes with fluorescent emitters, Nat. Commun. (2014), doi:http://dx.doi.org/10.1038/ncomms5016.
[15] C. Adachi, M.A. Baldo, M.E. Thompson, S.R. Forrest, Nearly 100% internal phosphorescence efficiency in an organic light-emitting device, J. Appl. Phys. 90 (2001) 5048.
[16] M.A. Baldo, C. Adachi, S.R. Forrest, Transient analysis of organic electro phosphorescence. II. Transient analysis of triplet-triplet annihilation, Phys. Rev. B 62 (2000) 10967.
[17] W.C. Wu, H.C. Yeh, L.H. Chan, C.T. Chen, Red organic light-emitting diode with a non-doping amorphous red emitter, Adv. Mater. 14 (2002) 1072–1075.
[18] S.C. Chang, G. He, F.C. Chen, T.F. Guo, Y. Yang, Degradation mechanism of phosphorescent-dye-doped polymer light-emitting diodes, Appl. Phys. Lett. 79 (2001) 2088–2090.
[19] G.Y. Zhong, Z. Xu, J. He, S.T. Zhang, Y.Q. Zhan, X.J. Wang, Z.H. Xiong, H.Z. Shi, X. M. Ding, W. Huang, X.Y. Hou, Aggregation and permeation of 4-(dicyanomethylene)-2-methyl-6-(p-dimethylaminostyryl)-4H-pyran molecules in Alq_3, Appl. Phys. Lett. 81 (2002) 1122–1124.
[20] J.R. Gong, L.J. Wan, S.B. Lei, C.L. Bai, Direct evidence of molecular aggregation and degradation mechanism of organic light-emitting diodes under joule heating: an STM and photoluminescence study, J. Phys. Chem. B 109 (2005) 1675–1682.
[21] P.I. Shih, C.Y. Chuang, C.H. Chien, E.W.G. Diau, C.F. Shu, Highly efficient non-doped blue-light-emitting diodes based on an anthrancene derivative end-capped with tetraphenylethylene groups, Adv. Funct. Mater. 17 (2007) 3141–3146.
[22] Y. Yuan, D. Li, X. Zhang, X. Zhao, Y. Liu, J. Zhang, Y. Wang, Phenanthroimidazole-derivative semiconductors as functional layer in high performance OLEDs, New J. Chem. 35 (2011) 1534–1540.
[23] K.C. Wu, P.J. Ku, C.S. Lin, H.T. Shih, F.I. Wu, M.J. Huang, J.J. Lin, I.C. Chen, C.H. Cheng, The photophysical properties of dipyrenylbenzenes and their application as exceedingly efficient blue emitters for electroluminescent devices, Adv. Funct. Mater. 18 (2008) 67–75.
[24] M.F. Wu, S.J. Yeh, C.T. Chen, H. Murayama, T. Tsuboi, W.S. Li, J.K. Wang, The quest for high-performance host materials for electrophosphorescent blue dopants, Adv. Funct. Mater. 17 (2007) 1887–1895.
[25] H. Huang, Q. Fu, S. Zhuang, Y. Liu, L. Wang, J. Chen, C. Yang, Novel deep blue OLED emitters with 1,3,5-Tri(anthracen-10-yl)-benzene-centered starburst oligofluorenes, J. Phys. Chem. C 115 (2011) 4872–4878.
[26] L. Xiao, S.J. Su, Y. Agata, H. Lan, J. Kido, Nearly 100% internal quantum efficiency in an organic blue-light electrophosphorescent device using a weak electron transporting material with a wide energy gap, Adv. Mater. 21 (2009) 1271–1274.
[27] H.H. Chou, C.H. Cheng, A highly efficient universal bipolar host for blue green, and red phosphorescent OLEDs, Adv. Mater. 22 (2010) 2468–2471.
[28] Y. Wang, X. Zhang, B. Han, J. Peng, H.H. Shiyou, Y. Huang, H. Sun, M. Xie, Z. Lu, The synthesis and photoluminescence characteristics of novel blue light-emitting naphthalimide derivatives, Dyes Pigm. 86 (2010) 190–196.
[29] T. Jairam, H. Ulla, M.N. Satyanarayan, V. Sivakumar, Synthesis, photophysical and electroluminescence studies of new triphenylamine-phenanthroimidazole based materials for organic light emitting diodes, J. Lumin. (2017), doi:http://dx.doi.org/10.1016/j.jlumin.2017.09.020.
[30] Z. Wang, C. Xu, W. Wang, X. Dong, B. Zhao, B. Ji, Novel pyrene derivatives: synthesis properties and highly efficient non-doped deep-blue electroluminescent device, Dyes Pigm. 92 (2011) 732–736.
[31] C.A. Wu, H.H. Chou, C.H. Shih, F.I. Wu, C.H. Cheng, H.L. Huang, T.C. Chao, M.R. Tseng, Synthesis and physical properties of meta-terphenyloxadiazole derivatives and their application as electron transporting materials for blue phosphorescent and fluorescent devices, J. Mater. Chem. 22 (2012) 17792–17799.
[32] Y.H. Lee, T.C. Wu, C.W. Liaw, T.C. Wen, S.W. Feng, J.J. Lee, Y.T. Wu, T.F. Guo, Non-doped active layer benzo[k]fluoranthene-based linear acenes, for deep blue- to green-emissive organic light-emitting diodes, Org. Electron. 14 (2013) 1064–1072.
[33] H. Ulla, B. Garudachari, M.N. Satyanarayan, G. Umesh, A.M. Isloor, Blue organic light emitting materials: synthesis and characterization of novel 1,8-naphthalimide derivatives, Opt. Mater. 36 (2014) 704–711.
[34] S.O. Jeon, S.E. Jang, H.S. Son, J.Y. Lee, External quantum efficiency above 20% in deep blue phosphorescent organic light-emitting diodes, Adv. Mater. 23 (2011) 1436.
[35] Y. Zhang, S.L. Lai, Q.X. Tong, M.F. Lo, T.W. Ng, M.Y. Chan, Z.C. Wen, J. He, K.S. Jeff, X.L. Tang, W.M. Liu, C.C. Ko, P.F. Wang, C.S. Lee, High efficiency nondoped deep-blue organic light emitting devices based on imidazole-π-triphenylamine derivatives, Chem. Mater. 24 (2012) 61–70.
[36] X. Yang, X. Yan, H. Guo, B. Liu, J. Zhao, G. Zhou, Y. Wu, Z. Wu b, W.-Y. Wong, Charged dinuclear Cu(I) complexes for solution-processed single-emitter warm white organic light-emitting devices, Dyes Pigm. 143 (2017) 151–164.
[37] X. Yang, Z. Feng, J. Zhao, J.-S. Dang, B. Liu, K. Zhang, G. Zhou, Pyrimidine-based mononuclear and dinuclear Iridium(III) complexes for high performance organic light-emitting diodes, ACS Appl. Mater. Interfaces 8 (2016) 33874–33887.
[38] H. Guo, J. Zhao, Z. Tian, Y. Wu, B. Liu, F. Dang, X. Yang, G. Zhou, Z. Wu, W.-Y. Wong, Homoleptic thiazole-based IrIII phosphorescent complexes for achieving both high EL efficiencies and an optimized trade-off among the key parameters of solution-processed WOLEDs, J. Mater. Chem. C 5 (2017) 208.
[39] J. Zhao, F. Dang, Z. Feng, B. Liu, X. Yang, Y. Wu, G. Zhou, Z. Wu, W.-Y. Wong, Highly efficient electroluminescent PtII ppy-type complexes with monodentate ligands, Chem. Commun. 53 (2017) 7581.
[40] J. Zhao, F. Dang, B. Liu, Y. Wu, X. Yang, G. Zhou, Z. Wu, W.-Y. Wong, Bis-ZnII salphen complexes bearing pyridyl functionalized ligands for efficient organic light-emitting diodes (OLEDs), Dalton Trans. 46 (2017) 6098.
[41] M.S. Subeesh, K. Shanmugasundaram, C.D. Sunesh, T.P. Nguyen, Y. Choe, Phenanthroimidazole derivative as an easily accessible emitter for non-doped light-emitting electrochemical cells, J. Phys. Chem. C 119 (2015) 23676–23684.
[42] D. Liu, M. Du, D. Chen, K. Ye, Z. Zhang, Y. Liu, Y. Wang, A novel tetraphenylsilane–phenanthroimidazole hybrid host material for highly efficient blue fluorescent, green and red phosphorescent OLEDs, J. Mater. Chem. C 3 (2015) 4394.
[43] X. Tang, Q. Bai, Q. Peng, Y. Gao, J. Li, Y. Liu, L. Yao, P. Lu, B. Yang, Y. Ma, Efficient deep blue electroluminescence with an external quantum efficiency of 6.8% and CIEy $<$0.08 based on a phenanthroimidazole-sulfone hybrid donor-acceptor molecule, Chem. Mater. 27 (2015) 7050.
[44] M. Chen, Y. Yuan, J. Zheng, W.C. Chen, L.J. Shi, Z.L. Zhu, F. Lu, Q.X. Tong, Q.D. Yang, J. Ye, M.Y. Chanand, C.S. Lee, Novel bipolar phenanthroimidazole derivative design for a nondoped deep-blue emitter with high singlet exciton yields, Adv. Opt. Mater. 3 (2015) 1215.
[45] Z. Wang, X. Li, K. Xue, H. Li, X. Zhang, Y. Liu, Z. Yu, P. Lu, P. Chen, Towards stable deep-blue emission and low efficiency roll-off in OLEDs based on phenanthroimidazole dimers, J. Mater. Chem. C 4 (2016) 1886.
[46] W. Qin, Z. Yang, Y. Jiang, J.W.Y. Lam, G. Liang, H.S. Kwok, B.Z. Tang, Construction of efficient deep blue aggregation-induced emission luminogen from triphenylethene for nondoped organic light emitting diodes, Chem. Mater. 27 (2015) 3892.
[47] Y. Yuan, J.X. Chen, F. Lu, Q.X. Tong, Q.D. Yang, H.W. Mo, T.W. Ng, F.L. Wong, Z.Q. Guo, J. Ye, Z. Chen, X.H. Zhang, C.S. Lee, Bipolar phenanthroimidazole derivatives containing bulky polyaromatic hydrocarbons for nondoped blue electroluminescence devices with high efficiency and low efficiency roll-off, Chem. Mater. 25 (2013) 4957.
[48] C. Hosokawa, H. Tokailin, H. Higashi, T. Kusumoto, Transient behavior of organic thin film electroluminescence, Appl. Phys. Lett. 60 (1992) 1220.
[49] M.S. Subeesh, K. Shanmugasundaram, C.D. Sunesh, T.P. Nguyen, Y. Choe, Phenanthroimidazole derivative as an easily accessible emitter for non-doped light-emitting electrochemical cells, J. Phys. Chem. C 119 (2015) 23676–23684.
[50] W.C. Chen, G.F. Wu, Y. Yuan, H.X. Wei, F.L. Wong, Q.X. Tong, C.S. Lee, A meta-molecular tailoring strategy towards an efficient violet-blue organic electroluminescent material, RSC Adv. 5 (2015) 18067–18074.
[51] K. Wang, S. Wang, J. Wei, Y. Miao, Z. Zhang, Z. Zhang, Y. Liu, Y. Wang, Structurally simple phenanthroimidazole-based bipolar hosts for high-

performance green and red electroluminescent devices, RSC Adv. 5 (2015) 73926–73934.
[52] Y.X. Wang, M.K. Leung, 4, 4′, 4″-Tris(acetoxymethylene)triphenylamine: an efficient photoacid promoted chemical cross-linker for polyvinylcarbozole and its applications for photolithographic hole-transport materials, Macromolecules 44 (2011) 8771–8779.
[53] W.C. Chen, Y. Yuan, G.F. Wu, H.X. Wei, J. Ye, M. Chen, F. Lu, Q.X. Tong, F.L. Wong, C.S. Lee, Molecular modification on bisphenanthroimidazole derivative for deep-blue organic electroluminescent material with ambipolar property and high performance, Org. Electron. 17 (2015) 159–166.
[54] S. Ebraheem, A.E. Saied, Band gap determination from diffuse reflectance measurements of irradiated lead borate glass system doped with TiO2 by using diffuse reflectance technique, Mater. Sci. Appl. 4 (2013) 324–329.
[55] P. Data, A. Kurowska, S. Pluczyk, P. Zassowski, P. Pander, R. Jedrysiak, M. Czwartosz, L. Otulakowski, J. Suwinski, M. Lapkowski, A.P. Monkman, Exciplex enhancement as a tool to increase OLED device efficiency, J. Phys. Chem. C 120 (2016) 2070–2078.
[56] H. Ulla, B. Garudachari, M.N. Satyanarayan, G. Umesh, A.M. Isloor, Blue organic light emitting materials: synthesis and characterization of novel 1 8-naphthalimide derivatives, Opt. Mater. 36 (2014) 704–711.
[57] J.C. Mello, H.F. Wittmann, R.H. Friend, An improved experimental determination of external photoluminescence quantum efficiency, Adv. Mater. 9 (1997) 230–232.
[58] G. Wu, F. Kong, Y. Zhang, X. Zhang, J. Li, W. Chen, W. Liu, Y. Ding, C. Zhang, B. Zhang, J. Yao, S. Dai, Multiple-anchoring triphenylamine dyes for dye-sensitized solar cell application, J. Phys. Chem. C 118 (2014) 8756–8765.
[59] K. Singh, R. Boddula, S. Vaidyanathan, Versatile luminescent europium(III)-β-diketonate-imidazo-bipyridyl complexes intended for white LEDs: a detailed photophysical and theoretical study, Inorg. Chem. 56 (2017) 9376–9390.
[60] A.B. Kajjam, S. Giri, V. Sivakumar, Triphenylamine-based donor-π-acceptor organic phosphors: synthesis, characterization and theoretical study, Mater. Chem. Front. 1 (2017) 512–520.
[61] J. Tagare, H. Ulla, A.B. Kajjam, M.N. Satyanarayan, S. Vaidyanathan, Star-shaped phenanthroimidazole-triphenylamine-based yellow organic emitter for organic light emitting diodes, ChemistrySelect 2 (2017) 2611–2620.
[62] M.J. Frisch, et al., Gaussian 09, Revision D.01, Gaussian, Inc., Wallingford, CT, 2009.
[63] D.M. Leeuw, M.M.J. Simenon, A.R. Brown, R.E.F. Einerhand, Stability of n-type doped conducting polymers and consequences for polymeric microelectronic devices, Synth. Met. 87 (1997) 53–59.
[64] Y. Tao, Q. Wang, L. Ao, C. Zhong, J. Qin, C. Yang, D. Ma, Molecular design of host materials based on triphenylamine/oxadiazoles hybrids for excellent deep-red phosphorescent organic light-emitting diodes, J. Mater. Chem. 20 (2010) 1759–1765.
[65] H. Ulla, M. Raveendra Kiran, B. Garudachari, T.N. Ahipa, A.V. Adhikari, Kartick Tarafder, M.N. Satyanarayan, G. Umesh, Blue emitting 1,8-naphthalimides with electron transport properties for organic light emitting diode applications, J. Mol. Struct. 1143 (2017) 344–354.
[66] S. Chidirala, H. Ulla, A. Valaboju, M.R. Kiran, M.E. Mohanty, M.N. Satyanarayan, G. Umesh, K. Bhanuprakash, V.J. Rao, Pyrene-oxadiazoles for organic light-emitting diodes: triplet to singlet energy transfer and role of hole-injection/hole-blocking materials, J. Org. Chem. 81 (2016) 603–614.
[67] Y.S. Park, S. Lee, K.H. Kim, S.Y. Kim, J.H. Lee, J.J. Kim, Exciplex-forming co-host for organic light-emitting diodes with ultimate efficiency, Adv. Funct. Mater. 23 (2013) 4914–4920.
[68] J. Kalinowski, Singlet generation from triplet excitons in fluorescent organic light-emitting diodes, Mater. Sci.-Poland 27 (2009) 735–756.
[69] Y.X. Wang, M.K. Leung, 4, 4′, 4″-Tris(acetoxymethylene)triphenylamine: an efficient photoacid promoted chemical cross-linker for polyvinylcarbozole and its applications for photolithographic hole-transport materials, Macromolecules 44 (2011) 8771–8779.
[70] X. Zhang, J. Lin, X. Ouyang, Y. Liu, X. Liu, Z. Ge, Novel host materials based on phenanthroimidazole derivatives for highly efficient green phosphorescent OLEDs, J. Photochem. Photobiol. A: Chem. 268 (2013) 37–43.
[71] C. Li, Z. Li, X. Yan, Y. Zhang, Z. Zhang, Y. Wang, Structurally simple non-doped sky-blue OLEDs with high luminance and efficiencies at low driving voltages, J. Mater. Chem. C 5 (2017) 1973–1980.